Original Article

Journal of Tissue Engineering
Volume 12: 1–14
© The Author(s) 2021
Article reuse guidelines:
sagepub.com/journals-permissions
DOI: 10.1177/20417314211021679
journals.sagepub.com/home/tej
SAGE

microRNA-129-5p shuttled by mesenchymal stem cell-derived extracellular vesicles alleviates intervertebral disc degeneration via blockade of LRG1-mediated p38 MAPK activation

Shaoqian Cui and Lei Zhang

Abstract

Mesenchymal stem cell (MSC)-derived extracellular vesicles (EVs) have been reported to deliver exogenous microRNAs (miRNAs or miRs) to reduce the progression of intervertebral disc degeneration (IDD). The purpose of the current study was to investigate the therapeutic potential of MSC-derived EVs delivering miR-129-5p in IDD. First, miR-129-5p expression levels were quantified in nucleus pulposus (NP) tissues of IDD patients. An IL-1β-induced NP cell model with IDD was then established, and co-cultured with EVs derived from MSCs that had been transfected with miR-129-5p mimic or inhibitor to elucidate the effects of miR-129-5p on cell viability, apoptosis, and ECM degradation. In addition, RAW264.7 cells were treated with the conditioned medium (CM) of NP cells. Next, the expression patterns of polarization markers and those of inflammatory factors in macrophages were detected using flow cytometry and ELISA, respectively. Lastly, rat models of IDD were established to validate the in vitro findings. It was found that miR-129-5p was poorly-expressed in NP tissues following IDD. Delivery of miR-129-5p to NP cells by MSC-derived EVs brought about a decrease in NP cell apoptosis, ECM degradation and M1 polarization of macrophages. Moreover, miR-129-5p directly-targeted LRG1, which subsequently promoted the activation of p38 MAPK signaling pathway, thus polarizing macrophages toward the M1 phenotype. Furthermore, MSC-derived EVs transferring miR-129-5p relieved IDD via inhibition of the LRG1/p38 MAPK signaling in vivo. Altogether, our findings indicated that MSC-derived EVs carrying miR-129-5p confer protection against IDD by targeting LRG1 and suppressing the p38 MAPK signaling pathway, offering a novel theranostic marker in IDD.

Keywords

Intervertebral disc degeneration, mesenchymal stem cells, extracellular vesicles, macrophages, microRNA-129-5p, LRG1, p38 MAPK signaling pathway

Date received: 25 December 2020; accepted: 14 May 2021

Introduction

Intervertebral disc degeneration (IDD) represents a multifactorial disease characterized by phenotypic and genotypic changes, leading to low back pain, and disability.[1] Once IDD occurs, intervertebral disc (IVD) tissues undergo inflammation, and this inflammation is often associated with a series of degenerative events which can precipitate discogenic pain.[2] Numerous causative factors for IDD have

Department of Spine Surgery, Shengjing Hospital of China Medical University, Shenyang, Liaoning, P.R. China

Corresponding author:
Lei Zhang, Department of Spine Surgery, Shengjing Hospital of China Medical University, No. 36, Sanhao Street, Heping District, Shenyang, Liaoning Province 110004, P.R. China.
Email: cmu_zl@163.com

been elucidated, such as genetic, biochemical and environmental factors, and lifestyles (aging, repetitive physical loading, obesity, and smoking), consequently causing an unbalance in the anabolic and catabolic environment of the extracellular matrix (ECM) favoring catabolism.[3] Current treatment approaches for IDD can provide symptomatic relief, but fail to resolve the underlying pathology of degeneration.[4] Accordingly, there is a pressing need to uncover novel molecular targets against IDD.

Mesenchymal stromal/stem cells (MSCs), a type of adult stem cells, are known to serve as promising candidates for numerous conditions, such as chronic degenerative disorders, inflammatory diseases, stroke, sepsis, or myocardial infarction.[5] Meanwhile, the paracrine functions of MSCs are exerted by secreting extracellular vesicles (EVs), which are predominantly endosomal in origin and contain various cargos, such as microRNAs (miRNAs or miRs), mRNAs, and proteins.[6] miRNAs, a class of small 18–22-nucleotide-long noncoding RNA molecules, have been previously highlighted to represent a promising approach for IDD management due to their ability to regulate nucleus pulposus (NP) cell viability, ECM synthesis, and apoptosis.[7] Furthermore, miR-129-5p can enhance cell viability, while inhibiting apoptosis of NP cells, thus contributing to the alleviation of IDD development by targeting BMP2.[8] Initial prediction results from the starBase database highlight the presence of miR-129-5p binding sites in the 3′-untranslated region (3′-UTR) of leucine-rich α2-glycoprotein1 (LRG1), a pleiotropic protein belonging to the LRG family that plays a pathogenic role in multiple degenerative diseases; for instance, accumulation of LRG is thought to be responsible for the neurodegeneration of patients with Parkinson's disease.[9] In addition, up-regulated expressions of LRG have been previously reported to be associated with granulomatous tissue formation, cartilage degeneration, and bone destruction in the event of rheumatoid arthritis.[10] Meanwhile, studies have also found that LRG1 exhibits a positive correlation with p38 mitogen-activated protein kinase (MAPK) signaling pathway in the setting of pancreatic cancer, wherein LRG1 promoted pancreatic cancer growth and metastasis by activating the signaling pathway.[11] On the other hand, p38 MAPK is known to be of paramount importance in the inflammatory response of NP cells, where cytokines mediated by p38 MAPK could induce the expression of catabolic enzymes a disintegrin-like and metalloproteinase domain with thrombospondin-type 1 motifs (ADAMTS) and matrix metalloproteinases (MMPs) in NP cells,[12] underscoring the significance of activated p38 MAPK signaling pathway in IDD. In lieu of these evidences, we hypothesize that MSCs-derived EV containing miR-129-5p may play a critical part in IDD via the LRG1/p38 MAPK axis. Consequently, the current study isolated EVs from human MSCs and conducted co-culture experiments with interleukin (IL)-1β-induced NP cells to verify this hypothesis, hoping to uncover effective therapeutic strategies combating IDD.

Materials and methods

Ethics statement

The current study was performed with the approval of the Ethic Committee of our hospital and performed in strict accordance with the *Declaration of Helsinki*. Signed informed consents were obtained from all participants prior to enrollment. Animal experiments were approved by the Ethic Committee of our hospital, and conformed to the Guide for the Care and Use of Laboratory Animals published by the US National Institutes of Health. Extensive efforts were made to ensure minimal suffering to the animals included in the study.

Clinical samples

Normal NP tissue samples were surgically collected from patients ($n = 30$, including 20 males and 10 females, aged 20–66 years, with a mean age of 42.4 years) with idiopathic scoliosis, and degenerative NP tissue samples were also collected from patients ($n = 30$, 19 males and 11 females, aged 26–55 years, with a mean age of 41.7 years) undergoing discectomy and spinal fusion. The obtained samples were graded using the Pfirrmann classification system.[13]

Isolation, culture, and treatment of NP cells

The collected NP tissue samples were sliced into small pieces and subjected to endonuclease cleavage with 0.2% type II collagenase (Invitrogen, Carlsbad, CA, USA) and 0.25% trypsin (Sigma-Aldrich Chemical Company, St Louis, MO, USA) for 3 h. Following rinsing with phosphate-buffered saline (PBS), the cells were separated with centrifugation. The isolated cells were subsequently cultured with Dulbecco's modified Eagle's medium (DMEM; Gibco, Grand Island, NY, USA) containing 15% fetal bovine serum (Gibco) and 1% penicillin-streptomycin solution in a 5% CO_2 incubator at 37°C. The culture medium was renewed twice a week, and the cells at passage 2 or 3 were used for follow-up experiments. Next, the cells were seeded in a 10-cm culture dish and allowed to reach 80% confluence, and then treated with 10 ng/mL of IL-1β for 24 h to construct a cell IDD model as previously described.[14]

Isolation and identification of BMSCs-derived EVs

Human BMSCs (acquired from American Type Culture Collection, Manassas, VA, USA) were cultured in serum-free DMEM and the culture solution was harvested after 2 days. Next, the cells were centrifuged at 500*g* for 10 min,

and 2000*g* for 30 min to remove the dead cells and cell debris. The supernatant was then collected and centrifuged at 100,000*g* and 4°C for 1 h, followed by suspension with phosphate buffer saline (PBS) and additional ultra-centrifugation as above mentioned. The obtained pellets were stored at −80°C.

The isolated EVs were then collected and observed under a transmission electron microscope (TEM; HT7830, Hitachi, Tokyo, Japan) for characterization. Briefly, EV suspension was mixed with equal volumes of 4% paraformaldehyde, and 5 μL of the mixture was loaded on the formvar/carbon coated copper grid, and the images were captured under a TEM.

Next, the diameter of EVs was detected by means of nanoparticles tracking analysis (NTA), which tracks and determines the particle size automatically based on Brownian motion and diffusion coefficient. EVs were then resuspended in 1 mL of PBS and filtered PBS served as a control. The diluted EVs were then injected into the NanoSight LM10 instrument (NanoSight Ltd., Minton Park, UK) to measure the particle size, with the condition set as 23.75°C ± 0.5°C for 60 s.

Subsequently, the surface marker proteins of EVs were identified using Western blot analysis. The EVs were then dissolved in radioimmunoprecipitation assay buffer and quantified with a bicinchoninic acid (BCA) protein assay kit (A53226, Thermo Fisher Scientific, Rockford, IL, USA). Next, the EVs were subjected to Western blot analysis with the following antibodies (Abcam Inc., Cambridge, UK): CD9 (ab92726, dilution ratio of 1: 1000), CD63 (ab134045, dilution ratio of 1: 1000), Calnexin (ab22595, dilution ratio of 1: 100) and TSG 101 (ab125011, dilution ratio of 1: 1000).

NP cell transfection

NP cells at the logarithmic growth phase were trypsinized and seeded into six-well plates at a density of 1×10^5 cells/well for 24 h of culture. Upon reaching approximately 75% confluence, the cells were then transfected with miR-129-5p mimic, miR-129-5p inhibitor, short hairpin RNA (sh)-LRG1, overexpression (oe)-LRG1, miR-129-5p mimic + LRG1 as well as their corresponding controls (mimic-negative control [NC], inhibitor-NC, control shRNA, oe-NC, miR-129-5p mimic + vector) according to the instructions of Lipofectamine 2000 reagent (Invitrogen). After 36 h of culture, the cells were treated with IL-1β and 10 μM of SB202190 (an inhibitor of p-38)[15] for 24 h. The aforementioned expression plasmids were purchased from Shanghai GenePharma Co., Ltd. (Shanghai, China) and the used concentration was 50 ng/mL.

Cell counting kit-8 (CCK-8) assay

NP cells were seeded into 96-well plates (Corning Incorporated, Corning, NY, USA) at a density of 2×10^3 cells/well (100 μL), and cultured overnight. Next, the cells were treated with 10 ng/mL of IL-1β for 24 h, and then co-cultured with BMSC-derived EVs for 3, 6, 9, and 12 days. Finally, 10 μL of CCK-8 reagent (K1018, Apexbio, USA) was added to each well at the corresponding time point, and incubated in dark conditions at 37°C for 2 h. The optical density (OD) values were measured at a wavelength of 450 nm. Five parallel wells were set for each experiment, with three independent repeats. A cell growth curve was finally plotted based on the viability.

Flow cytometry

The apoptosis rate of NP cells was measured using a Annexin V-allophycocyanin (APC) apoptosis detection kit (BD Pharmingen, San Diego, CA, USA). Briefly, the NP cells were resuspended in PBS and incubated with Annexin V-APC and propidium iodide (PI) in dark conditions at room temperature for 15 min. A FACScan flow cytometer (Becton Dickinson, San Diego, CA, USA) was used for cell apoptosis analysis.

Dual-luciferase reporter assay

LRG1-3′-UTR dual-luciferase reporter gene vectors (PmirGLO-LRG1-wild type (WT)) and mutant type (MUT) of LRG1 containing miR-129-5p binding sites (PmirGLO-LRG1-MUT) were constructed. Next, the reporter plasmids were co-transfected with miR-129-5p mimic or mimic NC plasmids into HEK-293T cells. After 48 h of transfection, the cells were lysed and centrifuged at 12,000*g* for 1 min, followed by supernatant collection. A Dual-Luciferase® Reporter Assay System (E1910, Promega Corporation, Madison, WI, USA) was employed to detect the luciferase activity, which was expressed as the ratio of firefly luciferase activity to renilla luciferase activity.

RNA isolation and quantitation

Total RNA content was extracted from tissues using the TRIzol reagent (16096020, Thermo Fisher Scientific Inc.). The extracted RNA was reverse-transcribed into complementary DNA (cDNA) using reverse transcription kits (RR047A, Takara, Japan, for mRNA detection), while polyA-tailing kits (B532451, Shanghai Sangon Biotechnology Co. Ltd., Shanghai, China, were employed for miRNA detection, containing universal PCR primer and U6 universal PCR primer). Reverse transcription quantitative polymerase chain reaction (RT-qPCR) was conducted using the SYBR® Premix Ex TaqTM II kit (DRR081, Takara, Japan) on an ABI 7500 instrument (Applied Biosystems, Foster City, CA, USA). Three wells were set for all experiments, each repeated in triplicate. U6 mRNA levels were used as an internal reference to normalize the results of miRNA expression, while syn-cel-miR-39 was used as the endogenous control for miRNA in EVs. In

addition, glyceraldehyde-3-phosphate dehydrogenase (GAPDH) served as the loading control of mRNAs. The primers are listed in Supplemental Table S1. The fold changes were calculated by means of relative quantification (the $2^{-\Delta\Delta Ct}$ method).

Western blot analysis

Total protein content was extracted from cells with radioimmunoprecipitation assay lysis buffer (P0013B, Shanghai Beyotime Biotechnology Co. Ltd., Shanghai, China). The concentration of the obtained proteins was then determined with a bicinchoninic acid (BCA) kit (A53226, Thermo Fisher Scientific, Rockford, IL, USA). Next, the proteins were separated using sodium dodecyl sulfate polyacrylamide gel electrophoresis and transferred onto polyvinylidene fluoride (IPVH85R, Millipore, Darmstadt, Germany) membranes using the wet-transfer method. Next, the membranes were blocked using 5% bovine serum albumin at ambient temperature for 1 h and underwent overnight incubation at 4°C with the following primary rabbit anti-human antibodies: collagen II (ab34712, dilution ratio of 1: 5000), aggrecan (13880-1-AP, dilution ratio of 1: 400), MMP-13 (ab39012, dilution ratio of 1: 4000), MMP3 (ab53015, dilution ratio of 1: 4000), p38 (ab227426, dilution ratio of 1: 500), phosphorylated (p)-p38 (ab38238, dilution ratio of 1: 500), and GAPDH (ab181602, dilution ratio of 1: 10000). The aforementioned antibodies were procured from Abcam Inc. (Cambridge, UK) except aggrecan (Proteintech, Wuhan, China). Following a wash, the membranes were re-probed with horseradish peroxidase-labeled secondary antibody to immunoglobulin G (IgG; ab6721, dilution ratio of 1: 5000, Abcam) for 2 h. The immunocomplexes on the membrane were visualized using chemiluminescence apparatus and band intensities were quantified with the ImageJ 1.48u software (National Institutes of Health, Bethesda, Maryland, USA). The ratio of the gray value of the target band to GAPDH was indicative of the relative protein expression.

Enzyme-linked immunosorbent assay (ELISA)

Macrophages were collected and centrifuged at 4°C, after which the supernatant was collected to determine the levels of cytokines with the help of ELISA. Briefly, the antibody was diluted to protein content of 1–10 μg/mL with 0.05 M carbonate-coated buffer (pH = 9). Next, 0.1 mL of the sample was added to the reaction well of each polystyrene plate, and reacted at 4°C overnight. The following day, the solution in the well was discarded and washed thrice with washing buffer solution. The coated reaction well was subsequently added with 0.1 mL of diluted samples to be tested and incubated at 37°C for 1 h. Following this, each well was added with 0.1 mL of fresh diluted enzyme labeled antibody and 0.1 mL of TMB substrate solution prepared temporarily, followed by reaction at 37°C for 10–30 min. The reaction was halted by the addition of 2 M sulfuric acid (0.05 mL). Finally, the optical density (OD) values of each well were measured at 450 nm using an ELISA detector.

Establishment of rat IDD models

A total of 24 male Sprague-Dawley rats (aged 3 months; calculated mean weight of 450 g ± 50 g) were enrolled in the study for in vivo experiments, among which, six rats were selected as the control (receiving sham operation) and the remaining 18 rats were used for IDD model construction.[16] In brief, the rats were deprived of food for 12 h and water for 4 h, and then peritoneally anesthetized with 3% sodium pentobarbital. Next, 2 IVDs (Co8/9 and Co9/10) were punctured using a 20-gauge needle. To ensure denaturation, the annulus fibrosus was punctured, the needle was rotated for 5 s and maintained for 30 s. In order to avoid the possible impact of individual differences, the IDD rats were treated with 100 μg/mL of EVs from mimic-NC-transfected MSCs or from miR-129-5p mimic-transfected MSCs, with six rats for each treatment. In total, 2 μL of sterile normal saline containing different purified cell EVs (about 1.5×10^6 granules) was injected into the central space of NP only at a depth of 6 μm. To avoid secondary damage caused by puncture, all injections were started 1 week after puncture. The puncture was repeated 4 weeks later.

Measurement of IVD index

The IVD index of each rat was examined by X-ray at the 1st, 5th, and 9th week before and after modeling. Prior to examination, the rats were anesthetized, and their limbs and tails were fixed in order to make tail muscle vertical and relaxed. The rats were scanned with a Faxitron Cabinet X-ray system (Faxitron Corp, Wheeling, IL), and the value of IVD height index (DHI) was obtained and calculated. The DHI value was expressed as percentage (%), which indicated the ratio of postoperative DHI to preoperative DHI.

Terminal deoxynucleotidyl transferase-mediated dUTP-biotin nick end labeling (TUNEL) assay

The tissue sections were dewaxed, rehydrated, and pretreated with proteinase K for 30 min. Next, the sections were balanced at 37°C for 1 h with the balance buffer of the kit, followed by incubation with peroxidase and diaminobenzidine. Finally, the sections were photographed under a microscope (Olympus, Tokyo, Japan).

Safranin-O/fast green staining

Paraffin sections were dewaxed with xylene I, II (5 min for each), and rehydrated with descending series of alcohol

(100%, 95%, 90%, 80%, and 70%, 3–5 min for each). Following washing with distilled water for 3 min, the sections were stained with Safranin dye for 10–30 min, and immersed with 1% hydrochloric acid ethanol for 2 s until the sections turned red with lighter color. Next, the sections were dehydrated with gradient alcohol (50%, 70%, and 80%) for 3–5 min. The sections were then counterstained and added with 95% ethanol to wash off the excess red, followed by immersion in absolute alcohol for 3–5 min. Finally, the sections were observed under a microscope following blocking with neutral gum.

Immunofluorescence staining

Sections were rinsed with PBS and blocked with 10% bovine serum albumin at 25°C for 1 h. Next, the sections were incubated with rabbit primary antibodies against iNOS (ab3523, dilution ratio of 1: 50, Abcam) and Arg1 (ab96183, dilution ratio of 1: 100, Abcam) in dark conditions at 4°C overnight. The following day, the sections were subjected to another round of incubation with fluorescent-labeled secondary antibody goat anti-rabbit IgG H&L (ab6717, dilution ratio of 1: 100, Abcam) at 37°C for 2 h. Following two rinses with PBS, the sections were stained with 4′,6-diamidino-2-phenylindole at room temperature for 15 min and observed under a confocal scanning microscopy (LSM 700; Carl Zeiss, Oberkochen, Germany).

Immunohistochemistry

Paraffin sections were baked at 60°C for 1 h, placed in xylene I and xylene II for dewaxing and hydration, dehydrated with gradient alcohol, and immersed in 3% hydrogen peroxide for 20 min at room temperature to terminate the endogenous peroxidase activity. Next, the sections were blocked with 10% goat serum for 15 min, incubated with diluted primary antibodies collagen II (ab34712, dilution ratio of 1: 5000, Abcam, Cambridge, UK), aggrecan (13880-1-AP, dilution ratio of e1:400, Proteintech, Wuhan, China), MMP13 (ab39012, dilution ratio of 1:4000, Abcam) and MMP3 (ab53015, dilution ratio of 1:4000, Abcam, Cambridge, UK), followed by overnight incubation at 4°C. The sections were then incubated with secondary antibody biotin-labeled goat anti-rabbit IgG working solution (ab97051, dilution ratio of 1: 2000, Abcam), incubated at room temperature for 40 min, and the color was developed with diaminobenzidine (DAB; DA1010, solarbio) for 10 min. Subsequently, the sections were counterstained with hematoxylin (H8070, Solarbio, Beijing, China) for 1 min, dried with gradient alcohol, transparentized with xylene and mounted with a gum. With PBS instead of primary antibody as the NC, the final results were scored by two double-blinded individuals. Five high-power fields were randomly selected under an optical microscope (CX41-12C02, Olympus, Tokyo, Japan). The cells presenting with brown particles in the cells were regarded as positive cells, and calculated as a percentage of the total number of cells.

Statistical analyses

Statistical analyses were performed using the SPSS 21.0 statistical software (IBM Corp. Armonk, NY, USA). Measurement data were described as mean ± standard deviation. Data obeying normal distribution and homogeneity of variance between two groups were compared using the unpaired *t*-test. Differences among multiple groups were statistically analyzed employing one-way analysis of variance (ANOVA) or repeated measures ANOVA, followed by Tukey's multiple comparisons test. The Kaplan-Meier method was used to calculate the survival rate of patients, and Log-rank test was used for univariate analysis. Correlation of indexes was analyzed by Pearson's correlation coefficient. A value of $p < 0.05$ was regarded statistically significant.

Results

miR-129-5p shuttled by BMSC-derived EVs inhibit cell apoptosis and the degradation of ECM in IL-1β-treated NP cells

Firstly, we set out to identify the isolated EVs from BMSCs. The results of TEM illustrated that the isolated EVs presented with round- or oval-shaped membranous vesicles (Figure 1(a)), and their size ranged 30–150 nm as evidenced by NTA (Figure 1(b)). In addition, Western blot analysis results demonstrated that the contents of EV surface makers CD9, CD63, and TSG101 were increased, while Calnexin was un-expressed (Figure 1(c)). These results indicated the successful extraction of EVs.

Differential analyses of the GSE19943 dataset indicated that miR-129-5p was poorly-expressed in IDD (Supplemental Figure S1A). In addition, the results of RT-qPCR demonstrated a decline in miR-129-5p expression levels in NP tissues of IDD patients (Figure 1(d)). Subsequently, MSCs were transfected with Cy3-labeled miR-129-5p mimic to obtain MSCs-EV with Cy3 labeled miR-129-5p. After incubating NP cells for 24 h (Figure 1(e)), red fluorescence was observed in NP cells co-cultured with EVs from BMSCs transfected with Cy3-labeled miR-129-5p mimic, indicating that miR-129-5p could be transferred from BMSC-derived EVs to NP cells (Figure 1(f)). Moreover, the results of RT-qPCR demonstrated that miR-129-5p expression levels were increased in NP cells with BMSC-EV-miR-129-5p mimic (Figure 1(g)). These results indicated that BMSCs-EV can transfer miR-129-5p into NP cells.

Furthermore, we over-expressed miR-129-5p in BMSCs, from which EVs were isolated. The results of RT-qPCR illustrated an increase in miR-129-5p expression

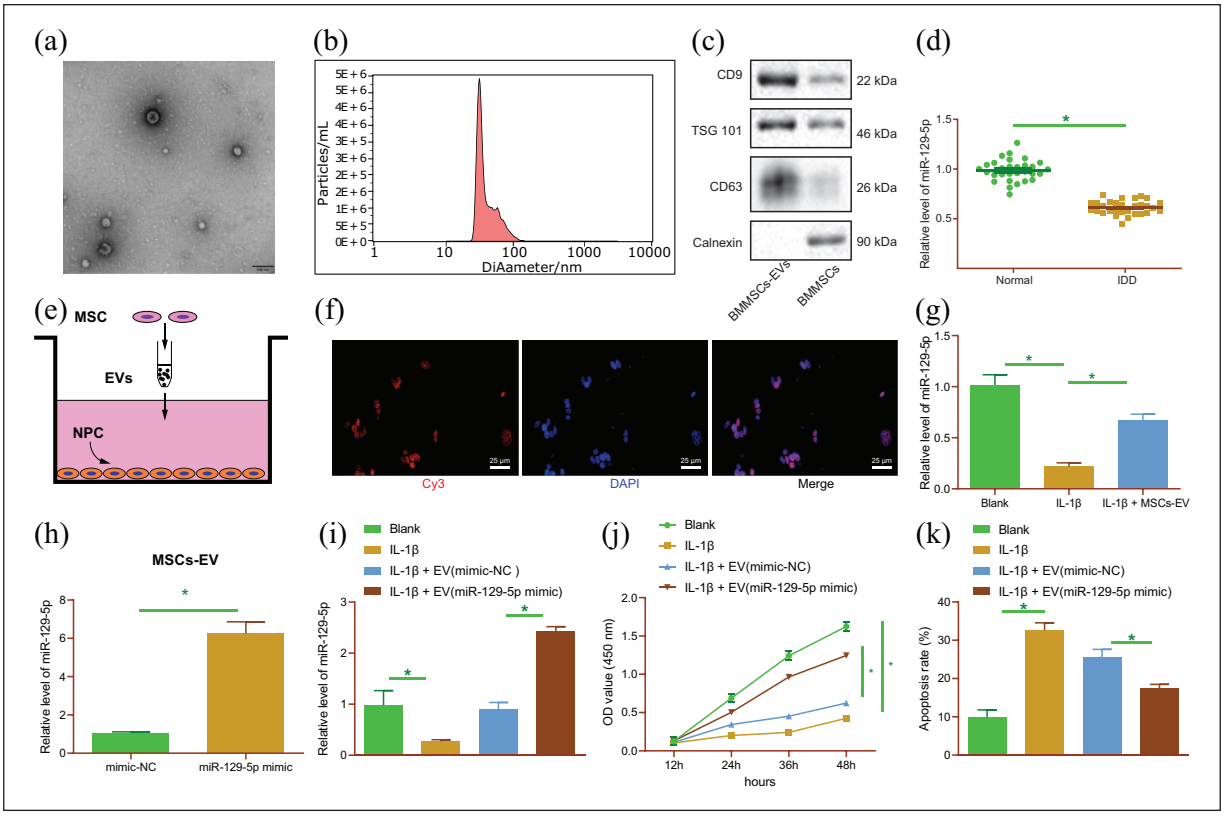

Figure 1. miR-129-5p delivered by BMSC-derived EVs inhibits IL-1β-treated NP cell apoptosis and ECM degradation in vitro. (a) Morphological characterization of EVs isolated from BMSCs observed under a TEM. (b) The size distribution of EVs analyzed by NTA. (c) Western blot analysis of EV surface maker proteins. (d) miR-129-5p expression determined by RT-qPCR in normal and IDD NP tissues ($n = 30$). (e) Schematic diagram of MSCs-EV incubating with NP cells. (f) Uptake of BMSC-EV from Cy3-labeled miR-129-5p by NP cells (scale bar = 25 μm). (g) miR-129-5p expression determined by RT-qPCR in NP cells with BMSC-EV-miR-129-5p mimic. (h) miR-129-5p expression determined by RT-qPCR in EVs from miR-129-5p-mimic-transfected BMSCs. IL-1β-induced NP cells were treated with EVs derived from miR-129-5p-mimic-transfected BMSCs. (i) miR-129-5p expression determined by RT-qPCR in cells. (j) viability of NP cells detected by CCK-8 assay. (k) Apoptosis of NP cells detected by flow cytometry. *$p < 0.05$. The experiment was run in triplicate independently.

levels in the EV (miR-129-5p mimic) (Figure 1(h)), suggesting the successful over-expression of miR-129-5p in BMSC-EVs. Next, we aimed to characterize the role of miR-129-5p carried by BMSCs-EVs in NP cells in vitro. NP cells were treated with IL-1β to simulate IDD in vitro, and then co-cultured with MSC-EVs with different treatments. Experimental data from RT-qPCR showed down-regulation of miR-129-5p in IL-1β-treated NP cells, while treatment with BMSC-EV-miR-129-5p mimic resulted in enhanced miR-129-5p expression levels (Figure 1(i)). The viability of NP cells (Figure 1(j)) treated with IL-1β was found to be reduced, while apoptosis (Figure 1(k); Supplemental Figure S1B) was enhanced. However, treatment with BMSC-EV-miR-129-5p mimic blocked the effect of IL-1β on the viability and apoptosis abilities of NP cells. Meanwhile, Western blot analysis revealed that the protein expression levels of collagen II and aggrecan were decreased in IL-1β-treated NP cells, while those of MMP13 and MMP3 were enhanced ($p < 0.05$), whereas these trends were reversed following co-culture with BMSC-EV-miR-129-5p mimic (Supplemental Figure S1C). These results highlighted the inhibitory potential of the BMSC-EVs containing miR-129-5p in the apoptosis of NP cells and the degradation of ECM during IDD.

miR-129-5p suppresses NP cell apoptosis, ECM degradation and M1 polarization of macrophages in vitro

Next, we proceeded to elucidate the relationship between miR-129-5p delivered by BMSC-derived EVs and macrophage polarization with IDD. First, we established NP cell IDD models using IL-1β, collected the conditioned medium (CM) of NP cells, and then treated RAW264.7 macrophages with the CM. The results of flow cytometry revealed higher expression levels of M1 marker CD86 and lower levels of M2 marker CD206 in the cells treated with CM of IL-1β-induced NP cells relative to control CM

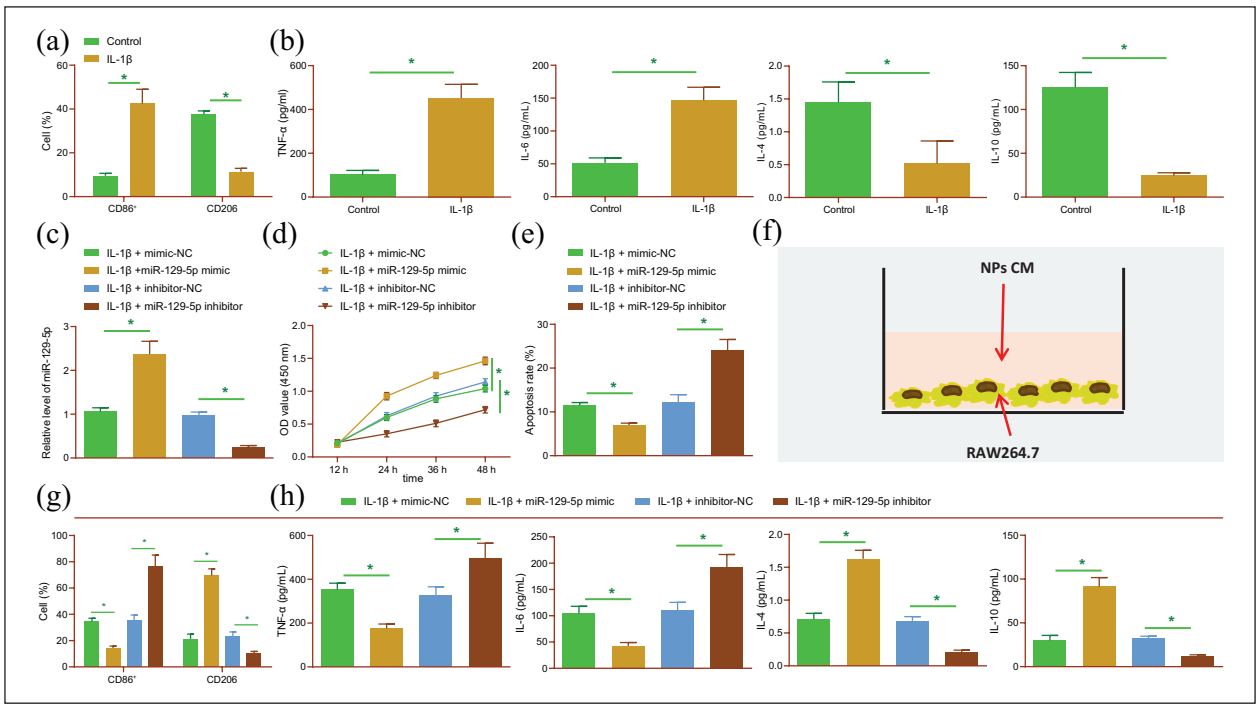

Figure 2. miR-129-5p represses cell apoptosis, ECM degradation and M1 polarization of macrophages in NP cells. (a) Flow cytometric analysis of expression of M1 marker CD86 and M2 marker CD206 in the RAW264.7 cells treated with CM of IL-1β-induced NP cells. (b) Expression of TNF-α, IL-6, IL-4, and IL-10 detected by ELISA in the RAW264.7 cells treated with CM of IL-1β-induced NP cells. IL-1β-induced NP cells were transfected with miR-129-5p mimic and miR-129-5p inhibitor. (c) Expression of miR-129-5p detected by RT-qPCR in NP cells. (d) Viability of NP cells detected by CCK-8 assay. (e) Apoptosis of NP cells detected by flow cytometry. (f) Schematic diagram of CM-treated RAW264.7 macrophages. (g) Flow cytometric analysis of expression of M1 marker CD86 and M2 marker CD206 in RAW264.7 cells. (h) Expression of TNF-α, IL-6, IL-4, and IL-10 detected by ELISA in RAW264.7 cells. *$p < 0.05$. The experiment was run in triplicate independently.

(Figure 2(a)). In addition, ELISA results illustrated that the expression levels of pro-inflammatory factors TNF-α and IL-6 were increased, while those of anti-inflammatory factors IL-4 and IL-10 were decreased in the presence of CM of IL-1β-induced NP cells (Figure 2(b)), indicating that degenerative NP cells can induce M1 polarization of macrophages.

As illustrated in Figure 2(c), RT-qPCR data demonstrated an enhancement in miR-129-5p expression levels in NP cells transfected with miR-129-5p mimic, while those treated with miR-129-5p inhibitor exhibited reduced expressions. Meanwhile, miR-129-5p mimic enhanced cell viability (Figure 2(d)), but diminished apoptosis (Figure 2(e); Supplemental Figure S2A); miR-129-5p inhibition brought about the opposite effects. Furthermore, the results of Western blot analysis demonstrated an increasing trend in the protein expression levels of collagen II and aggrecan, yet a decreasing trend in those of MMP13 and MMP3 following miR-129-5p mimic, which could be countered following miR-129-5p inhibition (Supplemental Figure S2B).

To further elucidate the effects of miR-129-5p on polarization of macrophages, we treated RAW264.7 macrophages with CM of NP cells (Figure 2(f)). Moreover, flow cytometric analysis illustrated decreased expression levels of CD86, while those of CD206 were increased in the RAW264.7 cells transfected with miR-129-5p mimic. Meanwhile, opposing trends were noted in the RAW264.7 cells transfected with miR-129-5p inhibitor (Figure 2(g)). Further, the expression levels of TNF-α and IL-6 were found to be decreased, while those of IL-4 and IL-10 were increased in response to miR-129-5p mimic, the effect of which was abrogated by miR-129-5p inhibitor (Figure 2(h)). Altogether, these results indicate that degenerative NP cells can promote M1 polarization of macrophages, and over-expression of miR-129-5p can inhibit the M1 polarization, apoptosis of NP cells, and ECM degradation.

miR-129-5p targets LRG1 and inhibits its expression in NP cells

After uncovering the inhibitory effect of miR-129-5p on NP cell apoptosis and M1 polarization of macrophages, we sought to further understand the underlying mechanism behind the inhibitory effect. The StarBase and mirDIP databases were searched to predict the downstream target genes of miR-129-5p, and the GSE124272 dataset was analyzed to predict the up-regulated genes in IDD. Subsequent results of intersection analysis revealed a total of 13 candidate target

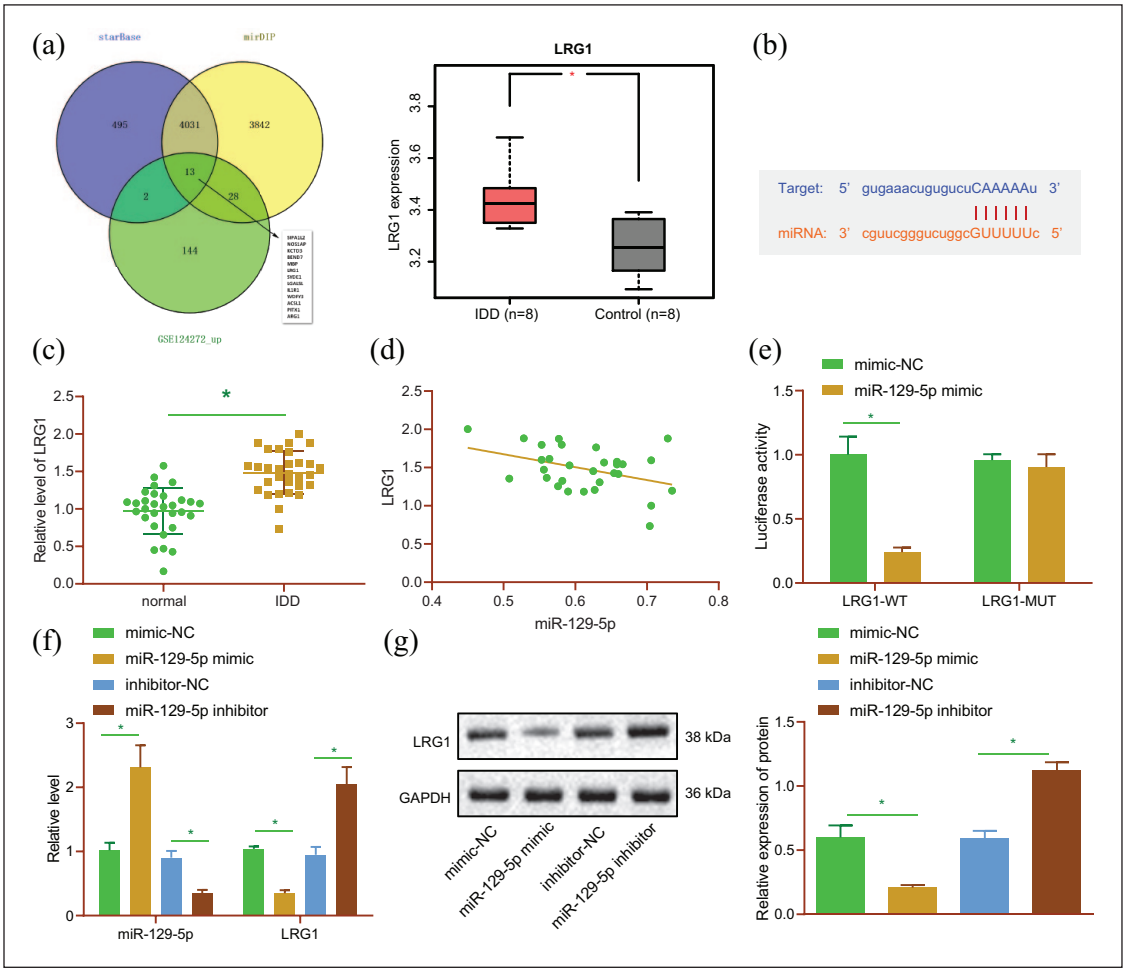

Figure 3. LRG1 is a target of miR-129-5p. (a) Venn diagram of the target genes of miR-129-5p predicted by the starBase and mirDIP databases, and upregulated genes in the GSE124272 dataset; expression of LRG1 in IDD in the GSE124272 dataset. (b) Putative miR-129-5p binding sites in the 3′UTR of LRG1 mRNA in the starBase website. (c) Expression of LRG1 detected by RT-qPCR in normal and NP tissues of 30 IDD patients. (d) Pearson correlation analysis of miR-129-5p expression with LRG1 in NP tissues. (e) Binding of miR-129-5p to LRG1 verified by dual-luciferase reporter assay in HEK-293T cells. (f) Expression of LRG1 detected by RT-qPCR in NP cells transfected with miR-129-5p mimic or inhibitor. (g) Western blot analysis of LRG1 protein in NP cells transfected with miR-129-5p mimic or inhibitor. *$p < 0.05$. The experiment was run in triplicate independently.

genes (Figure 3(a)). In addition, LRG1 expression patterns were detected, and found to be amplified in IDD tissues in the GSE124272 dataset (Figure 3(a)). In addition, the starBase website indicated the presence of miR-129-5p binding sites in the 3′UTR of LRG1 mRNA (Figure 3(b)). LRG1 was thus selected as the target for further analysis. Meanwhile, the results of RT-qPCR displayed up-regulated LRG1 expression levels in NP tissues of IDD patients relative to normal NP tissues (Figure 3(c)). An adverse correlation between miR-129-5p and LRG1 was further observed in NP tissues of IDD patients, as revealed by Pearson's correlation coefficient (Figure 3(d)). For further verification, dual luciferase reporter assay was performed, and it was found that the luciferase activity of LRG1-3′UTR-WT was decreased in HEK-293T cells transfected with miR-129-5p mimic ($p < 0.05$), while that of LRG1-3′UTR-MUT exhibited no difference ($p > 0.05$) (Figure 3(e)), indicating that miR-129-5p can specifically bind to 3′UTR of LRG1 gene. In addition, LRG1 expression levels were observed to be inhibited in NP cells transfected with miR-129-5p mimic, while being enhanced following miR-129-5p inhibition (Figure 3(f) and (g)). The aforementioned results suggested that miR-129-5p could inhibit LRG1 expression by targeting its 3′UTR in NP cells.

LRG1 promotes cell apoptosis, ECM degradation, and M1 polarization of macrophages by activating the p38 MAPK signaling pathway in NP cells

Numerous studies have indicated the critical role of p38 MAPK in inflammation of NP cells (Tian, Yuan 2013). In our study, the results of Western blot analysis showed that

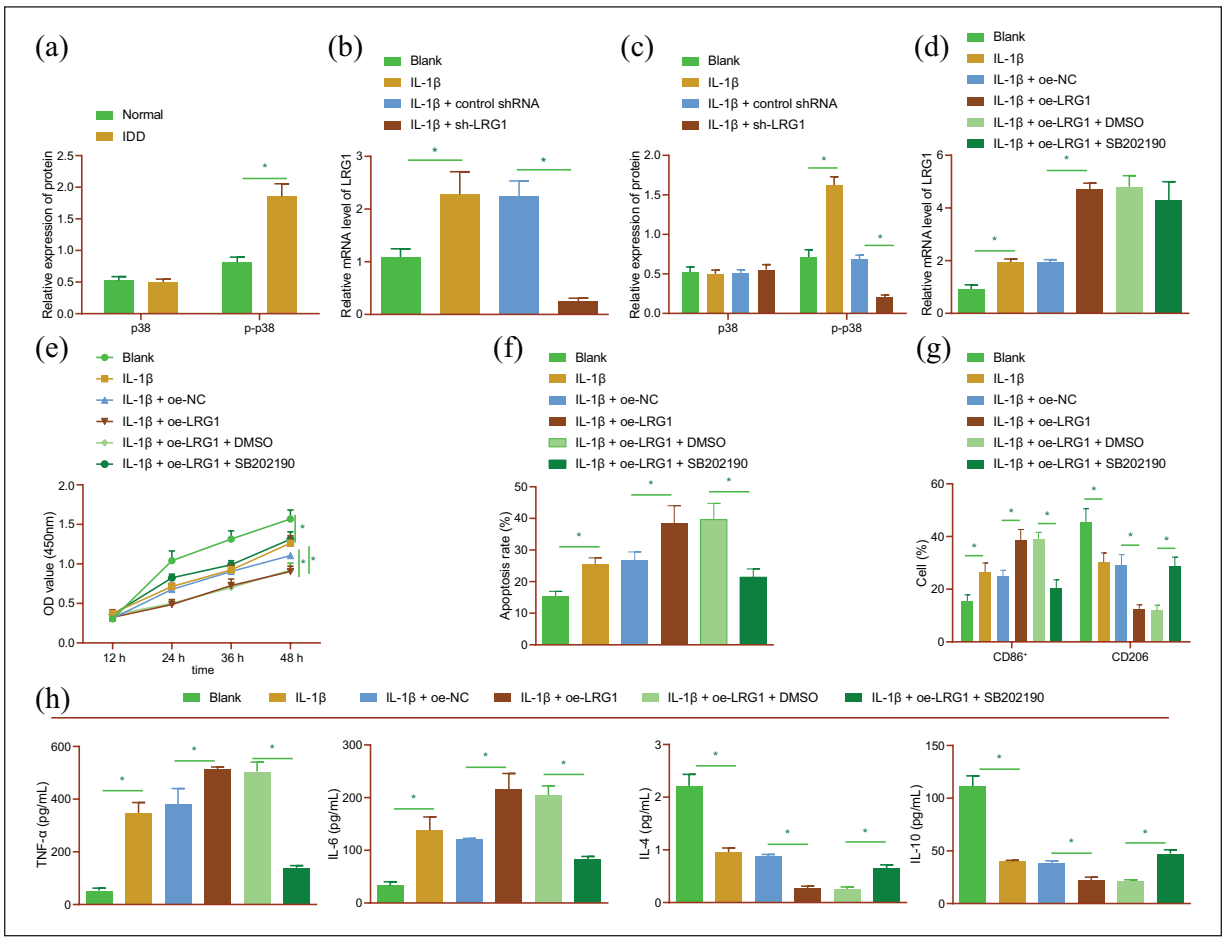

Figure 4. LRG1 facilitates cell apoptosis, ECM degradation, and M1 polarization of macrophages by activating the p38 MAPK signaling pathway in NP cells. (a) p38 phosphorylation level determined by Western blot analysis in normal and NP tissues of 30 IDD patients. (b) LRG1 mRNA expression detected by RT-qPCR in IL-1β-induced NP cells treated with sh-LRG1. (c) p38 phosphorylation level determined by Western blot analysis in IL-1β-induced NP cells treated with sh-LRG1. IL-1β-induced NP cells were treated with oe-LRG1 or in combination with SB202190. (d) LRG1 mRNA expression detected by RT-qPCR in NP cells. (e) Viability of NP cells detected by CCK-8 assay. (f) Apoptosis of NP cells detected by flow cytometry. (g) Flow cytometric analysis of expression of M1 marker CD86 and M2 marker CD206 in RAW264.7 cells. (h) Expression of TNF-α, IL-6, IL-4, and IL-10 detected by ELISA in RAW264.7 cells. *$p < 0.05$. The experiment was run in triplicate independently.

the extent of p38 phosphorylation was augmented in NP tissues of IDD patients (Figure 4(a); Supplemental Figure S3A). At the same time, RT-qPCR and Western blot analysis findings demonstrated an increase in LRG1 mRNA expression and p38 phosphorylation levels in IL-1β-treated NP cells, while silencing of LRG1 brought about the opposite results (Figure 4(b) and (c); Supplemental Figure S3B). These results suggested that silencing of LRG1 could reverse the activated p38 signaling pathway induced by IL-1β.

Furthermore, we explored the interaction between LRG1 and p38 MAPK in IDD, and found that the mRNA expression levels of LRG1 were elevated in IL-1β-treated NP cells, and similar trends were observed following LRG1 over-expression in IL-1β-treated NP cells (Figure 4(d)). In addition, cell viability was attenuated, while apoptosis was augmented upon IL-1β treatment; meanwhile, LRG1 over-expression resulted in more pronounced changes. Conversely, dual treatment with oe-LRG1 and SB202190 reduced cell apoptosis and potentiated the viability (Figure 4(e) and (f); Supplemental Figure S3C). Besides, the results of Western blot analysis indicated a decline in collagen II and aggrecan expression levels, yet an increase in those of MMP3 and MMP13 upon IL-1β treatment, the effect of which was further enhanced by LRG1 over-expression. However, treatment with both oe-LRG1 and SB202190 was found to bring about the opposite results (Supplemental Figure S3D). The aforementioned results demonstrated the promoting effect of LRG1 on cell apoptosis and ECM degradation by activating the p38 MAPK signaling pathway.

Subsequent analysis on the role of LRG1 in M1 polarization of macrophages was carried out using RAW264.7 cells treated with the CM of IL-1β-induced NP cells. Initially, flow cytometric analysis suggested that LRG1

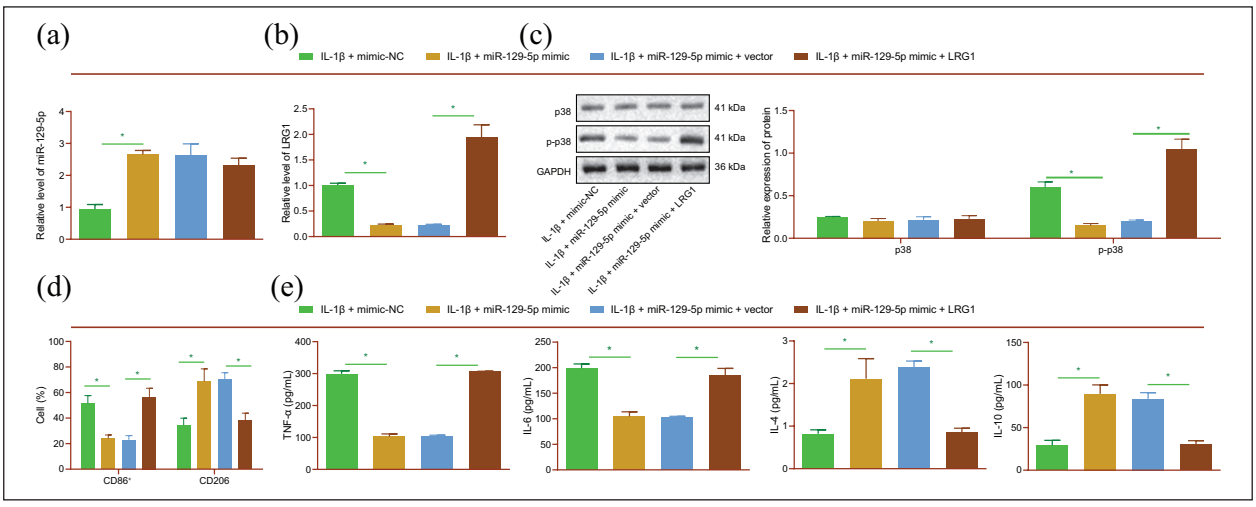

Figure 5. miR-129-5p attenuates the M1 polarization of macrophages via LRG1 downregulation in NP cells. IL-1β-induced NP cells were transfected with miR-129-5p mimic or in combination with LRG1. (a) miR-129-5p expression detected by RT-qPCR in NP cells. (b) LRG1 mRNA expression detected by RT-qPCR in NP cells. (c) p38 phosphorylation level determined by Western blot analysis in NP cells. RAW264.7 cells following treatment with the CM of IL-1β-induced NP cells were treated with miR-129-5p mimic or in combination with LRG1. (d) Flow cytometric analysis of expression of M1 marker CD86 and M2 marker CD206 in RAW264.7 cells. (e) Expression of TNF-α, IL-6, IL-4, and IL-10 detected by ELISA in RAW264.7 cells. $^*p < 0.05$. The experiment was run in triplicate independently.

over-expression brought about a more prominent elevation in CD86 expression levels, and a decline in CD206 expression following IL-1β treatment. Opposing trends were observed in the presence of both oe-LRG1 and SB202190 (Figure 4(g)). Besides, the increased expression levels of TNF-α and IL-6, and reduced IL-4 and IL-10 expression levels induced by IL-1β treatment were found to be more pronounced following over-expression of LRG1, the effect of which was undermined following oe-LRG1 and SB202190 in combination (Figure 4(h)). Collectively, these results indicated that LRG1 polarized macrophages toward M1 phenotype by activating the p38 MAPK signaling pathway in NP cells.

miR-129-5p delays M1 polarization of macrophages by targeting LRG1 in NP cells

We further performed mechanistic experiments to determine the effect of miR-129-5p on M1 polarization of macrophages by targeting LRG1 and the p38 MAPK signaling pathway. The results of RT-qPCR and Western blot analysis revealed up-regulated miR-129-5p expression levels in IL-1β-induced NP cells transfected with miR-129-5p mimic (Figure 5(a)). In addition, LRG1 mRNA expression and p38 phosphorylation levels were found to be decreased in the presence of miR-129-5p mimic, whereas further over-expression of LRG1 reversed this trend (Figure 5(b) and (c)). Meanwhile, miR-129-5p mimic was found to down-regulate the CD86 expression and up-regulate CD206 expression levels, which were negated by additional over-expression of LRG1 (Figure 5(d)). Moreover, treatment with miR-129-5p brought about a decrease in TNF-α and IL-6 expression levels, and enhanced those of IL-4 and IL-10 in response to miR-129-5p mimic, whereas opposite trends were evident in the presence of miR-129-5p mimic + LRG1 (Figure 5(e)). These results indicated that miR-129-5p suppressed the M1 polarization of macrophages in IL-1β-treated NP cells by targeting LRG1.

BMSC-derived EVs carrying miR-129-5p represses the M1 polarization of macrophages and relieves IDD by disrupting LRG1-dependent p38 MAPK activation in rats

Lastly, we focused our efforts to determine the effect of miR-129-5p carried by MSC-derived EVs on IDD in vivo. Rats were treated with EVs isolated from MSCs that had been transfected with miR-129-5p mimic or mimic-NC (Figure 6(a)). Subsequent results indicated that miR-129-5p was poorly-expressed, whereas LRG1 mRNA expression and p38 phosphorylation levels were increased in NP tissues of IDD rats. However, opposite trends were observed following over-expression of miR-129-5p (Figure 6(b) and (c); Supplemental Figure S4A). Meanwhile, the DHI of IDD rats was lower than that of sham-operated rats, while being increased in response to miR-129-5p over-expression (Figure 6(d)). In addition, the results of TUNEL and Safranin-O/fast green assays illustrated that cell apoptosis was increased and ECM degradation was severe in IDD rats, while miR-129-5p over-expression abolished these effects (Figure 6(e,f); Supplemental Figure S4B, C). Meanwhile, ECM-related proteins collagen II and aggrecan expression levels were decreased, while those of MMP13 and MMP3 were found

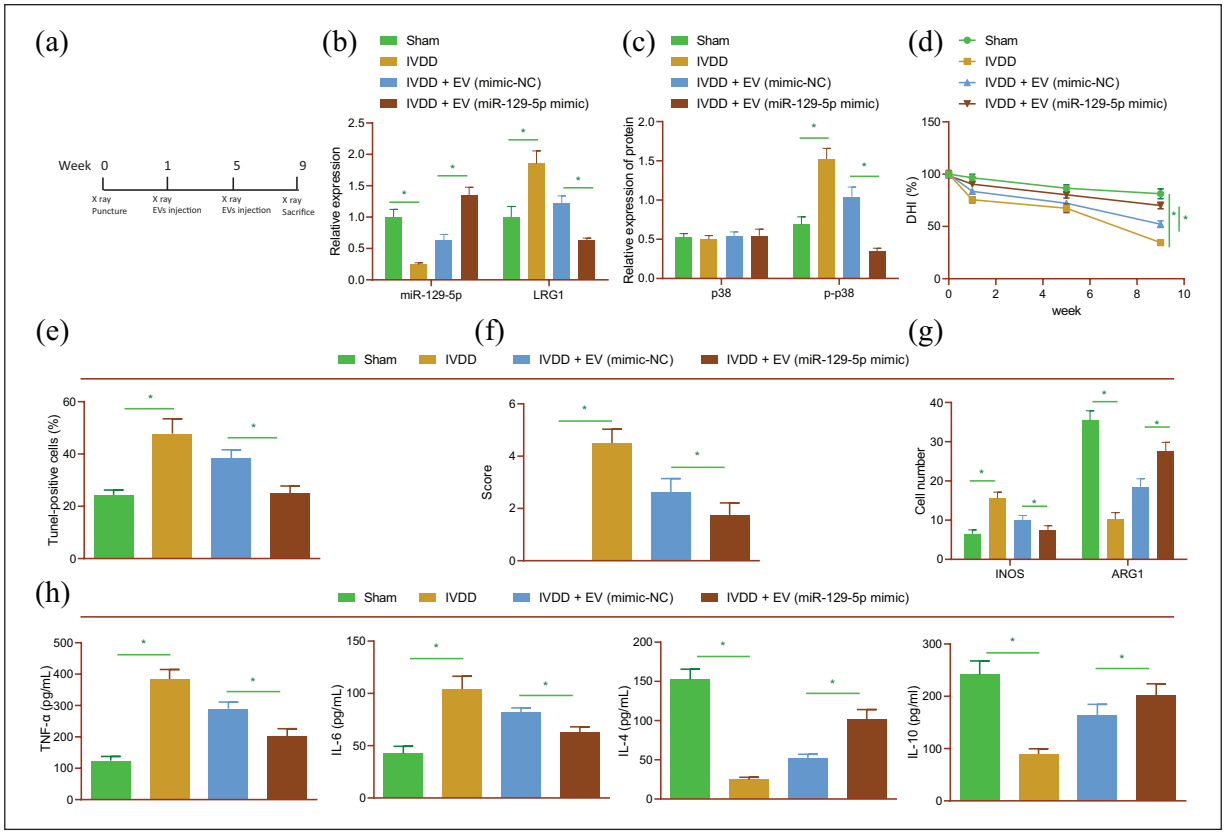

Figure 6. Delivery of miR-129-5p by BMSC-derived EVs blunts the M1 polarization of macrophages and retards the progression of IDD in vivo. Rats were treated with EVs isolated from BMSCs that had been transfected with miR-129-5p mimic. (a) Flow chart for in vivo experiment. (b) miR-217 expression and LRG1 mRNA expression detected by RT-qPCR in rat NP tissues. (c) p38 phosphorylation level determined by Western blot analysis in rat NP tissues. (d) DHI in rat NP tissues. (e) TUNEL staining of NP cell apoptosis in rat IVD tissues. (f) Safranin-O/fast green staining of ECM degradation in rat IVD tissues. (g) Immunofluorescence staining of M1 marker iNOS and M2 marker ARG1 in rat IVD tissues. (h) Expression of TNF-α, IL-6, IL-4, and IL-10 detected by ELISA in rat serum. $n = 8$ for rats upon each treatment. $^*p < 0.05$. The experiment was run in triplicate independently.

to be up-regulated in IDD rat tissues. On the other hand, treatment with miR-129-5p mimic brought about the opposite results (Supplemental Figure S4D).

Furthermore, treatment with miR-129-5p mimic was found to counteract the up-regulated M1 maker iNOS expression and down-regulated M2 maker ARG1 expression levels in IVD tissues of IDD rats (Figure 6(g); Supplemental Figure S4E). In addition, there were enhanced serum levels of TNF-α and IL-6, and diminished serum levels of IL-4 and IL-10 in IDD rats, while contrary trends were observed in the presence of miR-129-5p overexpression (Figure 6(h)). Altogether, the aforementioned results supported the notion that MSC-derived EVs carrying miR-129-5p could slow the M1 polarization of macrophages and ameliorate IDD by blocking LRG1-dependent p38 MAPK activation in rats.

Discussion

MSC-derived EVs are well-recognized as promising therapeutic agents against numerous human diseases owing to their ability to promote the process of tissue regeneration by creating a pro-regenerative environment enabling endogenous stem and progenitor cells to repair affected tissues.[17] Meanwhile, MSCs-EVs have been reported to inhibit allergic airway inflammation by immunomodulating pulmonary macrophages.[18] Dental pulp stem cells-EVs also enhance osteogenesis of adipose-derived stem cells via the MAPK pathway.[19] Stem cells-EVs enhances cartilage repair, which is benefit to protect the osteoarthritis joint from damage.[20] Expanding on existing data, findings obtained in the current study highlight the inhibitory effect of miR-129-5p shuttled by BMSC-derived EVs on the IDD progression via suppression of LRG1-dependent p38 MAPK signaling pathway activation.

Firstly, initial findings in our study illustrated that miR-129-5p shuttled by BMSC-derived EVs inhibited cell apoptosis and ECM degradation in IL-1β-treated NP cells. MSC-derived EVs are regarded as effective modulators of NP cell survival and apoptosis, which correlates to excessive endoplasmic reticulum stress in the IVD, in favor of IDD progression.[21,22] Meanwhile, previous studies have

also indicated the ability of MSC-derived EVs to promote ECM synthesis and viability, and reduce apoptosis in IVD cells.[23] More interestingly, the report by Zhai et al. demonstrated that human MSC-derived EVs enhance the process of bone regeneration by altering their miRNA cargos, including miR-129-5p.[24] Further in line with our results, other studies have also documented down-regulated expression levels of miR-129-5p in NP cells subjected to IDD.[25] Moreover, over-expression of miR-129-5p is known to potentiate viability, inhibit apoptosis, and up-regulate the expression of collagen II and aggrecan in NP cells of IDD rats, consequently improving the prognosis of IVD.[26] On the other hand, imbalances between ECM synthesis and degradation are regarded as the primary cause of IDD within the IVD, particularly in NP.[27] Furthermore, one particular study even highlighted ECM restoration as an effective strategy against IVD.[28] Up-regulated collagen II and aggrecan expressions, as well as inhibited MMP13 production have also been previously illustrated to contribute to alleviation of ECM degradation of NP cells.[27] These findings reveal that miR-129-5p shuttled by BMSC-derived EVs play a critical role in IVD

Meanwhile, the hard-done work of our peers further suggests that macrophages, a group of heterogeneous cells, play essential roles in physiological conditions and inflammatory responses.[29] Macrophages possess two major phenotypes: the pro-inflammatory M1 phenotype, and the anti-inflammatory M2 phenotype, such that the M1/M2 unbalance plays a pathogenic role in several human diseases.[30] In addition, polarization of M1 macrophages can precipitate local inflammation and structural change in the multifidus muscle following IDD.[31] Studies have also indicated that M1 macrophages promote the degenerative phenotypes in rat NP cells owing to their roles in augmenting the expression of key matrix catabolic genes (ADAMTS5, MMP3, and MMP13), and those of inflammation-related genes (IL-1β and IL-6), while reducing the expression of major matrix-associated anabolic genes (Sox9 and Col2a1).[32] Furthermore, the study by Yang et al. highlighted the property of miR-129-5p to reduce inflammatory responses in several conditions; for instance, the concentration of IL-6, IL-8, and TNF-α were previously found to be up-regulated in lipopolysaccharide-stimulated microglia following inhibition of miR-129-5p,[33] underscoring the inhibitory role of miR-129-5p in inflammatory response of microglia. Besides, up-regulation of miR-129-5p is also known to suppress the inflammatory reaction of neuronal cells following Alzheimer's disease.[33] In lieu of these findings, it would be plausible to suggest that miR-129-5p can inhibit the M1 polarization of macrophages, and thus suppress the progression of IDD.

Additionally, miRNAs are known to interact with the 3′UTR of specific target mRNAs, and consequently lead to the inhibition of their expression.[34] In our study, online biological prediction and luciferase reporter assay findings indicated that miR-129-5p bound to the 3′UTR of LRG1 mRNA, and subsequently inhibited its expression in NP cells. Moreover, LRG1 has been often over-expressed in multiple diseases.[35,36] Similarly, our findings demonstrated that LRG1 was highly-expressed in NP cells and tissues upon IDD. Meanwhile, a previous study revealed that LRG1 knockdown enhances osteoblast viability and collagen synthesis, and suppresses osteoblast apoptosis via promotion of the TGF-β1/SMAD signaling pathway in osteoporosis.[37] Further highlighting the significance of LRG in inflammation, increased serum levels of LRG were previously uncovered in lipopolysaccharide-mediated acute inflammation, whereas elevating TNF-α and IL-6 levels could induce LRG expression in ulcerative colitis COLO205 cells.[38] Remarkably, inhibition of LRG1 activity can contribute to the attenuation of degeneration of osteoarthritis articular cartilage in vivo.[39] Overall, the aforementioned data and findings indicate that miR-129-5p may cease NP cell apoptosis, ECM degradation, and M1 polarization of macrophages by targeting LRG1; however, due to the lack of available literature, the established mechanism requires further investigation.

Lastly, mechanistic investigation in our study demonstrated that BMSC-derived EVs carrying miR-129-5p repressed cell apoptosis, ECM degradation, and M1 polarization of macrophages by disrupting LRG1-dependent p38 MAPK activation, thus retarding the progression of IDD. Recent studies also suggest that LRG1 can augment the migration of thyroid carcinoma cells via activation of the p38 MAPK signaling pathway.[40] Furthermore, activation of p38 MAPK has been widely documented in IDD, and additionally, the production of GM-CSF and IFNγ caused by p38 in NP cells is known to polarize macrophages toward the M1 phenotype.[41] On the other hand, Anisomycin, a p38 MAPK signaling pathway activator, was previously highlighted to bring about a significant increase in compression-induced NP matrix degeneration and apoptosis,[42] which is largely consistent with the findings obtained in our study. More importantly, miR-129-3p down-regulation was shown to cause malignant phenotypes of hepatocellular cancer cells via activation of the p38 MAPK signaling pathway.[43]

Conclusion

Altogether, findings uncovered in our study indicate that BMSC-derived EVs transfer miR-129-5p to NP cells and perturb the apoptosis, ECM degradation and M1 polarization of macrophages by targeting LRG1 and inactivating the p38 MAPK signaling pathway, consequently alleviating the progression of IDD (Figure 7). Thus, BMSC-derived EV-mediated transfer of miR-129-5p could serve as potential effective biomarker for diagnosing and monitoring the progression of IDD.

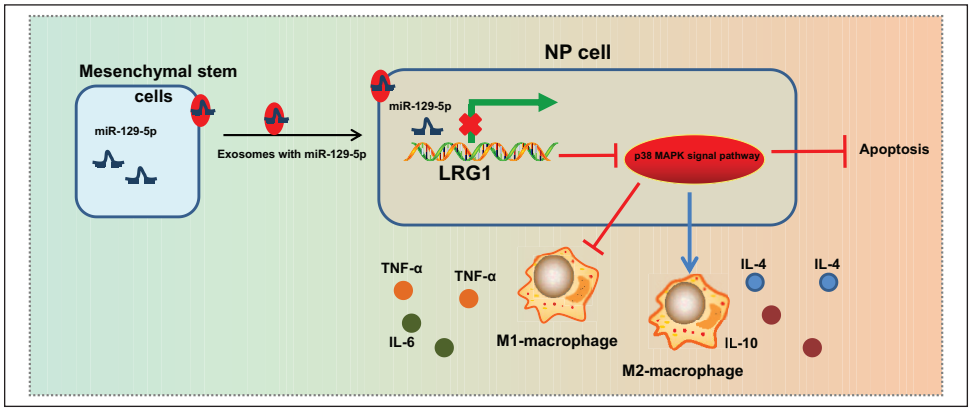

Figure 7. The mechanism graph of the regulatory network of BMSC-derived EVs delivering miR-129-5p in IDD. MSC-derived EVs deliver miR-129-5p to NP cells, which binds to 3′UTR of LRG1 to inhibit LRG1 expression, thus attenuating activation of the p38 MAPK signaling pathway. By this mechanism, miR-129-5p arrests M1 polarization of macrophages, while promoting M2 polarization to release anti-inflammatory factors, ultimately preventing NP cell apoptosis and alleviating IDD progression.

Acknowledgements

We would like to give our sincere appreciation to the reviewers for their helpful comments on this article.

Author contributions

Shaoqian Cui and Lei Zhang contributed to the conception and design of the study; Lei Zhang contributed to the acquisition of data; Shaoqian Cui and Lei Zhang contributed to the analysis and interpretation of data; Shaoqian Cui contributed to revising the article critically for important intellectual content; Shaoqian Cui and Lei Zhang approved the final version to be submitted.

Declaration of conflicting interests

The author(s) declared no potential conflicts of interest with respect to the research, authorship, and/or publication of this article.

Funding

The author(s) received no financial support for the research, authorship, and/or publication of this article.

ORCID iD

Lei Zhang https://orcid.org/0000-0002-4303-4943

Supplemental material

Supplemental material for this article is available online.

References

1. Wang SZ, Rui YF, Lu J, et al. Cell and molecular biology of intervertebral disc degeneration: current understanding and implications for potential therapeutic strategies. *Cell Prolif* 2014; 47(5): 381–390.
2. Navone SE, Marfia G, Giannoni A, et al. Inflammatory mediators and signalling pathways controlling intervertebral disc degeneration. *Histol Histopathol* 2017; 32(6): 523–542.
3. Dowdell J, Erwin M, Choma T, et al. Intervertebral disk degeneration and repair. *Neurosurgery* 2017; 80(3S): S46–S54.
4. Sampara P, Banala RR, Vemuri SK, et al. Understanding the molecular biology of intervertebral disc degeneration and potential gene therapy strategies for regeneration: a review. *Gene Ther* 2018; 25(2): 67–82.
5. Galipeau J and Sensebe L. Mesenchymal stromal cells: clinical challenges and therapeutic opportunities. *Cell Stem Cell* 2018; 22(6): 824–833.
6. Rani S, Ryan AE, Griffin MD, et al. Mesenchymal stem cell-derived extracellular vesicles: toward cell-free therapeutic applications. *Mol Ther* 2015; 23(5): 812–823.
7. Li Z, Yu X, Shen J, et al. MicroRNA in intervertebral disc degeneration. *Cell Prolif* 2015; 48(3): 278–283.
8. Yang W and Sun P. Downregulation of microRNA-129-5p increases the risk of intervertebral disc degeneration by promoting the apoptosis of nucleus pulposus cells via targeting BMP2. *J Cell Biochem* 2019; 120(12): 19684–19690.
9. Miyajima M, Nakajima M, Motoi Y, et al. Leucine-rich alpha2-glycoprotein is a novel biomarker of neurodegenerative disease in human cerebrospinal fluid and causes neurodegeneration in mouse cerebral cortex. *PLoS One* 2013; 8(9): e74453.
10. Fujimoto M, Serada S, Suzuki K, et al. Leucine-rich alpha2-glycoprotein as a potential biomarker for joint inflammation during anti-interleukin-6 biologic therapy in rheumatoid arthritis. *Arthritis Rheumatol* 2015; 67(8): 2056–2060.
11. Xie ZB, Zhang YF, Jin C, et al. LRG-1 promotes pancreatic cancer growth and metastasis via modulation of the EGFR/p38 signaling. *J Exp Clin Cancer Res* 2019; 38(1): 75.
12. Tian Y, Yuan W, Fujita N, et al. Inflammatory cytokines associated with degenerative disc disease control aggrecanase-1 (ADAMTS-4) expression in nucleus pulposus cells through MAPK and NF-kappaB. *Am J Pathol* 2013; 182(6): 2310–2321.
13. Song Y, Li S, Geng W, et al. Sirtuin 3-dependent mitochondrial redox homeostasis protects against AGEs-induced intervertebral disc degeneration. *Redox Biol* 2018; 19: 339–353.

14. Zhu L, Shi Y, Liu L, et al. Mesenchymal stem cells-derived exosomes ameliorate nucleus pulposus cells apoptosis via delivering miR-142-3p: therapeutic potential for intervertebral disc degenerative diseases. *Cell Cycle* 2020; 19(14): 1727–1739.
15. Ge J, Yan Q, Wang Y, et al. IL-10 delays the degeneration of intervertebral discs by suppressing the p38 MAPK signaling pathway. *Free Radic Biol Med* 2020; 147: 262–270.
16. Han B, Zhu K, Li FC, et al. A simple disc degeneration model induced by percutaneous needle puncture in the rat tail. *Spine (Phila Pa 1976)* 2008; 33(18): 1925–1934.
17. Borger V, Bremer M, Ferrer-Tur R, et al. Mesenchymal stem/stromal cell-derived extracellular vesicles and their potential as novel immunomodulatory therapeutic agents. *Int J Mol Sci* 2017; 18(7): 1450.
18. Fang SB, Zhang HY, Meng XC, et al. Small extracellular vesicles derived from human MSCs prevent allergic airway inflammation via immunomodulation on pulmonary macrophages. *Cell Death Dis* 2020; 11(6): 409.
19. Jin Q, Li P, Yuan K, et al. Extracellular vesicles derived from human dental pulp stem cells promote osteogenesis of adipose-derived stem cells via the MAPK pathway. *J Tissue Eng* 2020; 11: 2041731420975569.
20. Ni Z, Zhou S, Li S, et al. Exosomes: roles and therapeutic potential in osteoarthritis. *Bone Res* 2020; 8: 25.
21. Cheng X, Zhang G, Zhang L, et al. Mesenchymal stem cells deliver exogenous miR-21 via exosomes to inhibit nucleus pulposus cell apoptosis and reduce intervertebral disc degeneration. *J Cell Mol Med* 2018; 22(1): 261–276.
22. Liao Z, Luo R, Li G, et al. Exosomes from mesenchymal stem cells modulate endoplasmic reticulum stress to protect against nucleus pulposus cell death and ameliorate intervertebral disc degeneration in vivo. *Theranostics* 2019; 9(14): 4084–4100.
23. Piazza N, Dehghani M, Gaborski TR, et al. Therapeutic potential of extracellular vesicles in degenerative diseases of the intervertebral disc. *Front Bioeng Biotechnol* 2020; 8: 311.
24. Zhai M, Zhu Y, Yang M, et al. Human mesenchymal stem cell derived exosomes enhance cell-free bone regeneration by altering their miRNAs profiles. *Adv Sci (Weinh)* 2020; 7(19): 2001334.
25. Zhao K, Zhang Y, Kang L, et al. Methylation of microRNA-129-5P modulates nucleus pulposus cell autophagy by targeting Beclin-1 in intervertebral disc degeneration. *Oncotarget* 2017; 8(49): 86264–86276.
26. Li N, Gao Q, Zhou W, et al. MicroRNA-129-5p affects immune privilege and apoptosis of nucleus pulposus cells via regulating FADD in intervertebral disc degeneration. *Cell Cycle* 2020; 19(8): 933–948.
27. Vadala G, Ambrosio L, Russo F, et al. Interaction between mesenchymal stem cells and intervertebral disc microenvironment: from cell therapy to tissue engineering. *Stem Cells Int* 2019; 2019: 2376172.
28. Hodgkinson T, Wignall F, Hoyland JA, et al. High BMPR2 expression leads to enhanced SMAD1/5/8 signalling and GDF6 responsiveness in human adipose-derived stem cells: implications for stem cell therapies for intervertebral disc degeneration. *J Tissue Eng* 2020; 11: 2041731420919334.
29. Artyomov MN, Sergushichev A and Schilling JD. Integrating immunometabolism and macrophage diversity. *Semin Immunol* 2016; 28(5): 417–424.
30. Funes SC, Rios M, Escobar-Vera J, et al. Implications of macrophage polarization in autoimmunity. *Immunology* 2018; 154(2): 186–195.
31. James G, Sluka KA, Blomster L, et al. Macrophage polarization contributes to local inflammation and structural change in the multifidus muscle after intervertebral disc injury. *Eur Spine J* 2018; 27(8): 1744–1756.
32. Ni L, Zheng Y, Gong T, et al. Proinflammatory macrophages promote degenerative phenotypes in rat nucleus pulpous cells partly through ERK and JNK signaling. *J Cell Physiol* 2019; 234(5): 5362–5371.
33. Yang J, Sun G, Hu Y, et al. Extracellular vesicle lncRNA metastasis-associated lung adenocarcinoma transcript 1 released from glioma stem cells modulates the inflammatory response of microglia after lipopolysaccharide stimulation through regulating miR-129-5p/high mobility group box-1 protein axis. *Front Immunol* 2019; 10: 3161.
34. Ali Syeda Z, Langden SSS, Munkhzul C, et al. Regulatory mechanism of MicroRNA expression in cancer. *Int J Mol Sci* 2020; 21(5): 1723.
35. Hong Q, Wang S, Liu S, et al. LRG1 may accelerate the progression of ccRCC via the TGF-beta pathway. *Biomed Res Int* 2020; 2020: 1285068.
36. Jin J, Sun H, Liu D, et al. LRG1 promotes apoptosis and autophagy through the TGFbeta-smad1/5 signaling pathway to exacerbate ischemia/reperfusion injury. *Neuroscience* 2019; 413: 123–134.
37. Gu Z, Xie D, Huang C, et al. MicroRNA-497 elevation or LRG1 knockdown promotes osteoblast proliferation and collagen synthesis in osteoporosis via TGF-beta1/Smads signalling pathway. *J Cell Mol Med* 2020; 24(21): 12619–12632.
38. Serada S, Fujimoto M, Terabe F, et al. Serum leucine-rich alpha-2 glycoprotein is a disease activity biomarker in ulcerative colitis. *Inflamm Bowel Dis* 2012; 18(11): 2169–2179.
39. Wang Y, Xu J, Zhang X, et al. TNF-alpha-induced LRG1 promotes angiogenesis and mesenchymal stem cell migration in the subchondral bone during osteoarthritis. *Cell Death Dis* 2017; 8(3): e2715.
40. Ban Z, He J, Tang Z, et al. LRG1 enhances the migration of thyroid carcinoma cells through promotion of the epithelial–mesenchymal transition by activating MAPK/p38 signaling. *Oncol Rep* 2019; 41(6): 3270–3280.
41. Yang C, Cao P, Gao Y, et al. Differential expression of p38 MAPK alpha, beta, gamma, delta isoforms in nucleus pulposus modulates macrophage polarization in intervertebral disc degeneration. *Sci Rep* 2016; 6: 22182.
42. Liu W, Jin S, Huang M, et al. Duhuo jisheng decoction suppresses matrix degradation and apoptosis in human nucleus pulposus cells and ameliorates disc degeneration in a rat model. *J Ethnopharmacol* 2020; 250: 112494.
43. Cui S, Zhang K, Li C, et al. Methylation-associated silencing of microRNA-129-3p promotes epithelial-mesenchymal transition, invasion and metastasis of hepatocelluar cancer by targeting Aurora-A. *Oncotarget* 2016; 7(47): 78009–78028.